


## Article

# Formation and Photophysical Properties of Silver Clusters in Bulk of Photo-Thermo-Refractive Glass

Leonid Yu. Mironov <sup>1,\*</sup> , Dmitriy V. Marasanov <sup>1</sup>, Mariia D. Sannikova <sup>1</sup>, Ksenia S. Zyryanova <sup>1</sup>, Artem A. Slobozhaninov <sup>1</sup> and Ilya E. Kolesnikov <sup>2</sup>

<sup>1</sup> Research and Educational Center for Photonics and Optoinformatics, ITMO University, Kronverkskiy Pr. 49, Saint Petersburg 197101, Russia

<sup>2</sup> Center for Optical and Laser materials research, St. Petersburg University, 7/9 Universitetskaya Nab, Saint Petersburg 199034, Russia

\* Correspondence: leonid\_mironov@itmo.ru

**Abstract:** The bright luminescence of silver clusters in glass have potential applications in solid-state lighting, optical memory, and spectral converters. In this work, luminescent silver clusters were formed in the bulk of photo-thermo-refractive glass (15Na<sub>2</sub>O-5ZnO-2.9Al<sub>2</sub>O<sub>3</sub>-70.3SiO<sub>2</sub>-6.5F, mol.%) doped with different Ag<sub>2</sub>O concentrations from 0.01 to 0.05 mol.%. The spontaneous formation of plasmonic nanoparticles during glass synthesis was observed at 0.05 mol.% of Ag<sub>2</sub>O in the glass composition, limiting the silver concentration range for cluster formation. The luminescence of silver clusters was characterized by steady-state and time-resolved spectroscopy techniques. The rate constants of fluorescence, phosphorescence, intersystem crossing, and nonradiative deactivation were estimated on the basis of an experimental study. A comparison of the results obtained for the photophysical properties of luminescent silver clusters formed in the ion-exchanged layers of photo-thermo-refractive glass is provided.

**Keywords:** glass; luminescence; silver clusters



**Citation:** Mironov, L.Y.; Marasanov, D.V.; Sannikova, M.D.; Zyryanova, K.S.; Slobozhaninov, A.A.; Kolesnikov, I.E. Formation and Photophysical Properties of Silver Clusters in Bulk of Photo-Thermo-Refractive Glass. *Ceramics* **2023**, *6*, 1546–1558. <https://doi.org/10.3390/ceramics6030096>

Academic Editors: Anna Lukowiak, Georgiy Shakhgildyan and Michael I. Ojovan

Received: 30 May 2023

Revised: 5 July 2023

Accepted: 6 July 2023

Published: 13 July 2023



**Copyright:** © 2023 by the authors. Licensee MDPI, Basel, Switzerland. This article is an open access article distributed under the terms and conditions of the Creative Commons Attribution (CC BY) license (<https://creativecommons.org/licenses/by/4.0/>).

## 1. Introduction

Functional optical materials based on silver clusters have found different applications in white light generation [1], optical data storage [2–4], sensing [5,6], spectral conversion [7], waveguides [8–10], and radiation measurements [11,12]. Currently, the development of new materials for effective solid-state lighting is attracting a lot of attention because of its potential to reduce electricity consumption. White light generation with silver clusters was achieved through the combination of a blue light-emitting diode (LED) with a layer of organic ligand-stabilized Ag<sub>6</sub> clusters with a quantum yield of 95% at room temperature [13]. Although the emission of Ag<sub>6</sub> clusters was shown to be thermally stable, the combined emission of blue LED and Ag<sub>6</sub> showed a significant drop near 500 nm, which is similar to the widely applied cerium-doped yttrium aluminum garnet (YAG:Ce) luminophore [14].

Luminescent silver clusters in inorganic hosts, such as zeolites and glasses, have great potential as light-emissive materials for white LEDs. Silver cluster-doped materials possess broad emission spectra, covering the whole visible spectrum under long-wave ultraviolet (UV) excitation around 365 nm, which is available from commercial LEDs. Unlike traditional luminophores, such as rare-earth-doped or transition metal-doped crystal powders, silver clusters have no distinguished emission bands, providing natural lighting with a high color-rendering index. Luminescent materials based on silver clusters in zeolites were shown to have intense green-yellow luminescence with a quantum yield of 83% in Linde Type A (LTA) zeolites [15–17] and up to 100% in faujasite (FAU) zeolites [18]. Although zeolite-based materials are established as promising materials for white light emission, their long-term stability may be affected by the sorption properties of zeolites.

It was shown that the external quantum efficiency of silver clusters in LTA, FAUX, and FAUY zeolites fell 1.1–10 times after one month in a high-humidity environment [19]. Unlike zeolites, inorganic glass provides excellent chemical stability for silver clusters dispersed in the bulk of glass. The use of oxyfluoride glass doped with silver was proposed to generate white light with different color temperatures under near-UV irradiation [20]. Recently, a prototype of a white LED was realized by a combination of a UV LED with peak emission at 365 nm and silver clusters dispersed in borosilicate glass. The prototype was characterized by color coordinates of (0.32, 0.37) and a color rendering index of 89.7, indicating that silver clusters dispersed in inorganic glass have the potential for white light generation [21].

Silicate glasses have been used to host luminescent silver clusters because of their chemical and mechanical stability. Also, it was shown that in silica-based glass, silver clusters can have a quantum yield of luminescence up to 63% [22]. There are three main methods to introduce silver ions into silicate glass: the addition of silver compounds to a glass batch, ion exchange, and ion implantation. The most straightforward approach is the addition of silver compounds to the glass batch, leading to the formation of silver clusters in the bulk of the material. Since the solubility of silver ions in silica glasses is low, the main limitation of this approach is the spontaneous aggregation of luminescent silver clusters into larger non-luminescent silver species, such as plasmonic nanoparticles [23]. The ion exchange method modifies the surface layer of the glass after synthesis; it is necessary to introduce alkali metal ions into the glass composition to exchange them with silver ions by immersing them in a silver-containing salt melt. It is possible to introduce >10 mol.% of Ag<sub>2</sub>O into silicate glass by tuning the glass composition, the time and temperature of ion exchange, and the salt melt composition [24]. Additionally, ion exchange is an established method of optical waveguide production [25]. The thickness of an ion exchange layer depends on the exact parameters of the process and reaches several tens of micrometers. Similar to ion exchange, ion implantation also introduces silver ions only into the surface layer of the glass, but the thickness of the modified layer is usually less than two micrometers [26,27]. Also, ion implantation requires more complicated equipment in comparison with other methods.

In this work, we synthesized luminescent silver clusters in the bulk of photo-thermo-refractive glass and extensively studied their luminescent properties using steady-state and time-resolved spectroscopy. Earlier, the formation of luminescent silver clusters was shown in the bulk of glass with a similar composition, but the optical characterization lacked the study of luminescence quantum yields as well as fluorescence and phosphorescence decay kinetics [23]. Furthermore, the comparison of photophysical properties with the properties of silver clusters synthesized using the ion exchange technique in similar glass was performed. It was shown that although the concentration of Ag<sup>+</sup> was 200–500 times larger for the ion-exchanged glasses, the photophysical properties of the silver clusters were close. This result supports the suggestion that only small silver clusters, consisting of only 2–4 atoms, are luminescent.

## 2. Materials and Methods

Photo-thermo-refractive glass with the composition 15Na<sub>2</sub>O-5ZnO-2.9Al<sub>2</sub>O<sub>3</sub>-70.3SiO<sub>2</sub>-6.5F (mol.%) was used to form luminescent clusters in the bulk of the glass. The glass matrix was additionally doped with 0.02 mol.% of Sb<sub>2</sub>O<sub>3</sub> and 0.007 mol.% of CeO<sub>2</sub>. The concentrations of Ag<sub>2</sub>O were 0.01, 0.025, and 0.05 mol.%, corresponding to the samples Ag.01, Ag.025, and Ag.05. The glass was synthesized in a quartz ceramic (stekrit) crucible at 1440 °C in an air atmosphere, and a platinum stirrer was used to homogenize the glass melt. The glass transition temperature ( $T_g$ ) of the samples was measured with an STA 449 F1 Jupiter (Netzsch) differential scanning calorimeter at a heating rate of 10 K/min, and  $T_g$  was found to be 486 °C. Glass samples were cut in plates with a thickness of ~1 mm and further polished for spectroscopy analysis. To initiate cluster formation, the glass samples were irradiated with a mercury lamp for 10 min on each side and subsequently

heat-treated. Irradiation was necessary to ionize  $\text{Ce}^{3+}$  into  $\text{Ce}^{4+}$ , and the released electrons were trapped by  $\text{Sb}^{5+}$  ions forming  $(\text{Sb}^{5+})^-$  species. The time of irradiation was chosen to ensure the saturation of  $\text{Ce}^{3+}$  ionization. Further heat treatment provided energy to release electrons from  $(\text{Sb}^{5+})^-$  and reduce  $\text{Ag}^+$  ions to  $\text{Ag}^0$ , followed by cluster formation. The mechanism of photo-thermo-induced crystallization in the PTR glass has been studied in detail previously [28,29]. The heat treatment of the irradiated glass samples was carried out at 350, 400, and 450 °C for three hours.

Absorption spectra were measured using a PerkinElmer Lambda 650 spectrophotometer. Steady-state emission spectra and absolute quantum yields of luminescence were acquired using a Hamamatsu C9920 setup equipped with a 150 W CW xenon lamp, an 8.3 cm integrating sphere, and a PMA-12 CCD spectrometer. Time-resolved emission spectra were measured using a PerkinElmer LS50B fluorometer equipped with a pulsed xenon lamp with a pulse width at half maximum < 10  $\mu\text{s}$ . The fluorometer was used in the phosphorescence measurement mode, which made it possible to record sample emission with a fixed delay time after the excitation pulse. Total emission spectra representing combined fluorescence and phosphorescence of silver clusters were measured without delay after the excitation pulse. Further, the phosphorescence of silver clusters was detected with a delay of 40  $\mu\text{s}$  after the excitation pulse to ensure full decay of the excitation pulse; the value of the delay time was established according to the scattering reference. The fluorescence spectra were reconstructed by subtracting the phosphorescence spectra from the total emission spectra. Steady-state and time-resolved spectra were measured under 340 nm excitation; the second order diffraction peak from excitation pulse was blocked with a cut-off filter. All spectra were corrected for the sensitivity of the detector. Fluorescence decay curves were obtained with a HORIBA Fluorolog-3 fluorometer using the time-correlated single photon counting (TCSPC) technique, and fluorescence was excited by an LED at 340 nm with a 1.2 ns pulse. The experimental decay curves were fitted using bi-exponential or tri-exponential functions, depending on the goodness of the fit. Average fluorescence lifetimes were obtained using the following equation in the case of the bi-exponential fitting:

$$\tau_{\text{avg}} = \frac{\alpha_1 \tau_1^2 + \alpha_2 \tau_2^2}{\alpha_1 \tau_1 + \alpha_2 \tau_2}, \quad (1)$$

where  $\alpha_i$  is the amplitude of the  $i$ -th component, and  $\tau_i$  is the lifetime of the  $i$ -th component. Average fluorescence lifetimes in the case of triexponential fitting were calculated using the following equation:

$$\tau_{\text{avg}} = \frac{\alpha_1 \tau_1^2 + \alpha_2 \tau_2^2 + \alpha_3 \tau_3^2}{\alpha_1 \tau_1 + \alpha_2 \tau_2 + \alpha_3 \tau_3}, \quad (2)$$

where  $\alpha_i$  is the amplitude of the  $i$ -th component, and  $\tau_i$  is the lifetime of the  $i$ th component. Phosphorescence decay curves were obtained using phosphorescence spectra recorded with different delays after the excitation pulse and a fixed gate time.

### 3. Results and Discussion

Silica-based glasses have a low solubility of silver ions, which limits the concentration of  $\text{Ag}_2\text{O}$  introduced through the glass batch. Absorption spectra of the initial glass samples are shown in Figure 1a, demonstrating that the Ag.01 and Ag.025 samples were transparent in the visible range. A characteristic absorption band of  $\text{Ce}^{3+}$  ions was observed at 310 nm for all samples with the contribution of  $\text{Ce}^{4+}$  ions in the shorter wavelength region [30]. Additionally, the Ag.05 sample had an intense absorption peak at 410 nm corresponding to the plasmon absorption of silver nanoparticles. Therefore, spontaneous formation of silver nanoparticles during the synthesis of glass with the  $\text{Ag}_2\text{O}$  concentration of 0.05 mol.% was observed for the studied glass system. UV irradiation of the glass samples with a mercury lamp induced the appearance of additional unstructured absorption caused by the transition of cerium ions to the  $\text{Ce}^{4+}$  state (Figure 1b–d) and a decrease in the intensity of  $\text{Ce}^{3+}$  absorption bands as a result of photoionization. The increase in absorption originated

from a tail of the strong charge transfer transition of  $Ce^{4+}$  in the near-UV region, since  $Ce^{4+}$  has a  $4f^0$  configuration and, therefore, cannot exhibit f-f or f-d transitions [31]. Further heat treatment had a different effect on the samples with different  $Ag_2O$  concentrations. The Ag.01 sample demonstrated the formation of typical unstructured absorption of silver clusters between 320 and 400 nm after heat treatment at 350 °C (Figure 1b). An increase in the heat treatment temperature to 400 and 450 °C led to the appearance of distinguishable absorption peaks of silver nanoparticles. It is interesting that the Ag.025 sample with a higher silver concentration demonstrated the appearance of silver nanoparticles only after heat treatment at 450 °C (Figure 1c). The Ag.05 sample retained the shape and position of the plasmon peak after UV irradiation and heat treatment (Figure 1d). The formation of unstructured absorption overlapping with the plasmon peak is attributed to the appearance of luminescent silver clusters, since it was shown further that Ag.05 glass samples possess efficient emission after heat treatment.

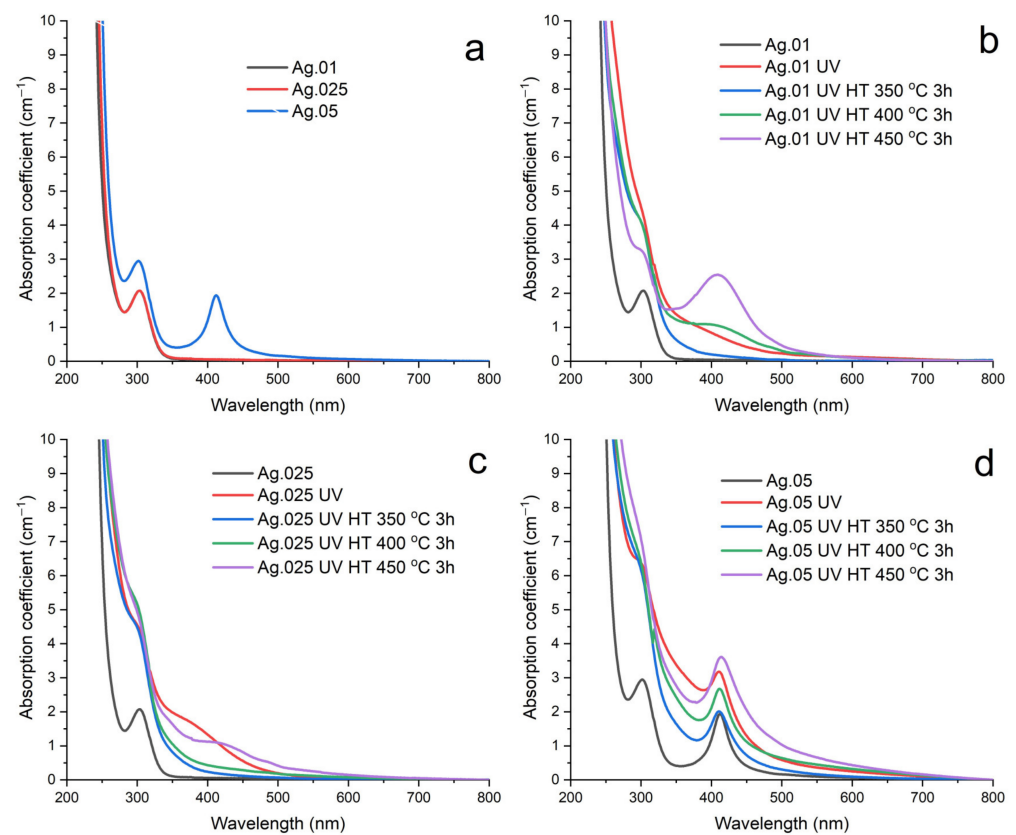


**Figure 1.** Comparison of initial glass absorption spectra (a). Influence of UV irradiation and heat treatment on the absorption of Ag.01 (b), Ag.025 (c), and Ag.05 (d) glass samples.

The calculation of the effective optical size of silver nanoparticles was carried out according to the Mie theory [32,33] using the following equation:

$$d = (2\nu F) / \Delta w, \quad (3)$$

where  $d$  is the average silver nanoparticle diameter,  $\nu F$  is the Fermi velocity ( $1.39 \times 10^8$  cm/s for silver [34]), and  $\Delta w$  is the full width at half maximum (FWHM) in angular frequency units. The results of the nanoparticle size calculation for the samples with distinguishable plasmon peaks are shown in Table 1. It can be seen that the increase in the concentration of  $Ag_2O$  in glass composition led to the formation of larger nanoparticles.

The initial samples of photo-thermo-refractive glass demonstrated luminescence under 340 nm excitation originating from the set of glass dopants. Normalized luminescence spectra of Ag.01, Ag.025, and Ag.05 samples are shown in Figure 2a. It can be seen that Ag.01 and



Ag.025 glasses had very similar luminescence, consisting of a single band corresponding to the emission of  $\text{Ce}^{3+}$  [35,36]. The fluorescence decay curves of Ag.01 and Ag.025 samples were fitted with a tri-exponential function (Figure 2b); the corresponding average fluorescence lifetimes were 23.7 and 28.3 ns. The Ag.05 luminescence spectrum differed significantly from those of the Ag.01 and Ag.025 glasses; an increase in the  $\text{Ag}_2\text{O}$  concentration led to the appearance of a broad luminescence signal in the range of 425–700 nm (Figure 2a). Time-resolved spectroscopy revealed that the additional emission from the Ag.05 sample was mostly long-lived phosphorescence with a maximum at 510 nm and a lifetime of 100  $\mu\text{s}$  (Figure 2c). Comparison of the short-lived emission spectra of Ag.05 and Ag.01 shows that the fluorescence of Ag.05 was wider and tailed more to the longer wavelength region (Figure 2d). The combination of fluorescence and phosphorescence with emission in blue and green-yellow parts of the spectra is a characteristic feature of the luminescence of silver clusters in the studied glass matrix [24,37]. Additionally, we observed a decrease in the fluorescence lifetime to 16.9 ns, which may originate from the contribution of silver clusters, since the fluorescence lifetime of silver clusters in the studied glass varies from 3.2 to 4.5 ns. Therefore, the formation of luminescent silver species together with plasmonic nanoparticles was observed after the synthesis and annealing of Ag.05 glass.

**Table 1.** Size of silver nanoparticles calculated via Mie theory.

Heat Treatment Temperature, °C	Ag.01	Ag.025	Ag.05
Initial glass	-	-	6 nm
350	-	-	6 nm
400	1 nm	-	6 nm
450	2 nm	4 nm	6 nm

The initial samples of Ag.01, Ag.025, and Ag.05 glasses had a relatively low luminescence quantum yield ranging from 0.06 to 0.1, which decreased by a factor of 2–5 to 0.02–0.05 after UV irradiation (Table 2). The decrease in the luminescence quantum efficiency after UV irradiation corresponded to the transition of  $\text{Ce}^{3+}$  to  $\text{Ce}^{4+}$ , which is generally non-luminescent [38]. UV irradiation of the initial glass samples also changed the shape of the luminescence spectra. Comparison of Figure 2a,e shows that the contribution of the  $\text{Ce}^{3+}$  emission peak to the glass luminescence was minimized with the increasing concentration of  $\text{Ag}_2\text{O}$  in the glass; the simultaneous appearance of a broad emission band with a maximum at 580 nm was observed. This emission band should belong to some transition species in the glass formed under the UV irradiation, rather than to luminescent clusters. The maximum of silver clusters' phosphorescence was located at shorter wavelengths near 540–550 nm (Figure 3). Also, the broad emission band at 580 nm decayed mainly during the time of excitation flash from the xenon lamp; phosphorescence was only a small fraction of the total emission from the UV-irradiated Ag.025 sample (Figure 2f). Additionally, it was assumed earlier that the main electron acceptors at the stage of UV irradiation of photo-thermo-refractive glass are  $\text{Sb}^{5+}$  ions, which form  $(\text{Sb}^{5+})^-$  centers and donate the trapped electrons to  $\text{Ag}^+$  ions only during further heat treatment [39].

The UV-irradiated samples of Ag.01, Ag.025, and Ag.05 glasses were heat treated at 350, 400, and 450 °C for 3 h to initiate the intense formation of silver clusters. After heat treatment, the glass samples demonstrated bright white emission under UV excitation (Figure 4a). The quantum yield of luminescence increased from 0.02–0.05 to a maximum value of 0.43 for the Ag.05 sample after heat treatment at 400 °C. After heat treatment, the luminescence spectra of the glass samples demonstrated continuous emission from 400 to 720 nm (Figure 3), except the Ag.01 glass after the heat treatment at 450 °C, for which luminescence was mainly in the red part of the spectrum (Figure 3c). Using time-resolved spectroscopy, the emission of glass samples was separated into fluorescence and phosphorescence with lifetimes of several nanoseconds and hundreds of microseconds, respectively. The coexistence of fluorescence and phosphorescence is a specific feature of the

silver cluster emission in glasses and was observed earlier for a similar glass system with silver clusters formed using the  $\text{Na}^+\text{-Ag}^+$  ion exchange technique [40]. It can be seen that, for all concentrations of  $\text{Ag}_2\text{O}$  in glass, an increase in the heat treatment temperature led to a decrease in the fluorescence contribution to the total emission spectra. This tendency partly originates from the reabsorption of cluster emission, but cannot be totally attributed to the inner-filter effect, considering that the absorption spectra of Ag.025 glass heat treated at 350 and 400 °C were almost identical (Figure 1c), while the contribution of fluorescence lowered from 37% to 28% of the total light emission. Additionally, only for Ag.05 glass samples with the most prominent plasmon peak of silver nanoparticles, we observed a clear reabsorption mark at 410 nm (Figure 3g–i). Therefore, changes in the fluorescence to phosphorescence ratio should originate from the formation of different sets of luminescent silver clusters after heat treatment at different temperatures.

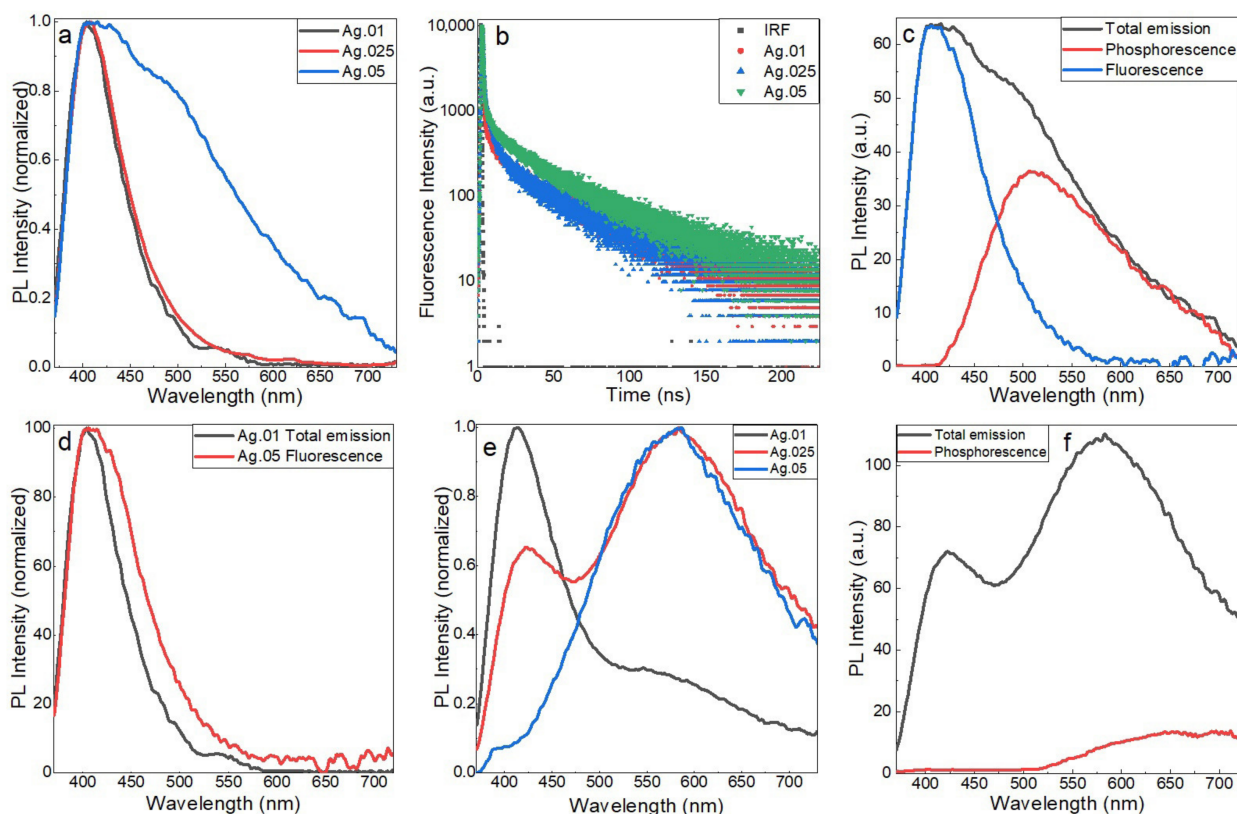


**Figure 2.** Normalized luminescence spectra of the initial glass samples,  $\lambda_{\text{ex}} = 340$  nm (a). Fluorescence decay curves of the initial glass samples registered at 405 nm,  $\lambda_{\text{ex}} = 340$  nm (b). Fluorescence, phosphorescence, and total emission spectra of the initial Ag.05 glass sample,  $\lambda_{\text{ex}} = 340$  nm (c). Comparison of the Ag.01 and Ag.05 glass fluorescence spectra,  $\lambda_{\text{ex}} = 340$  nm (d). Normalized luminescence spectra of the glass samples after UV irradiation,  $\lambda_{\text{ex}} = 340$  nm (e). Phosphorescence and total emission spectra of the Ag.025 glass after UV irradiation,  $\lambda_{\text{ex}} = 340$  nm (f).

**Table 2.** Quantum yields of Ag.01, Ag.025, and Ag.05 glass samples under 340 nm excitation.

Heat Treatment Temperature, °C	Ag.01	Ag.025	Ag.05
Initial glass	0.1	0.06	0.09
UV-irradiated initial glass	0.02	0.03	0.05
350	0.25	0.35	0.34
400	0.16	0.42	0.43
450	0.07	0.32	0.3

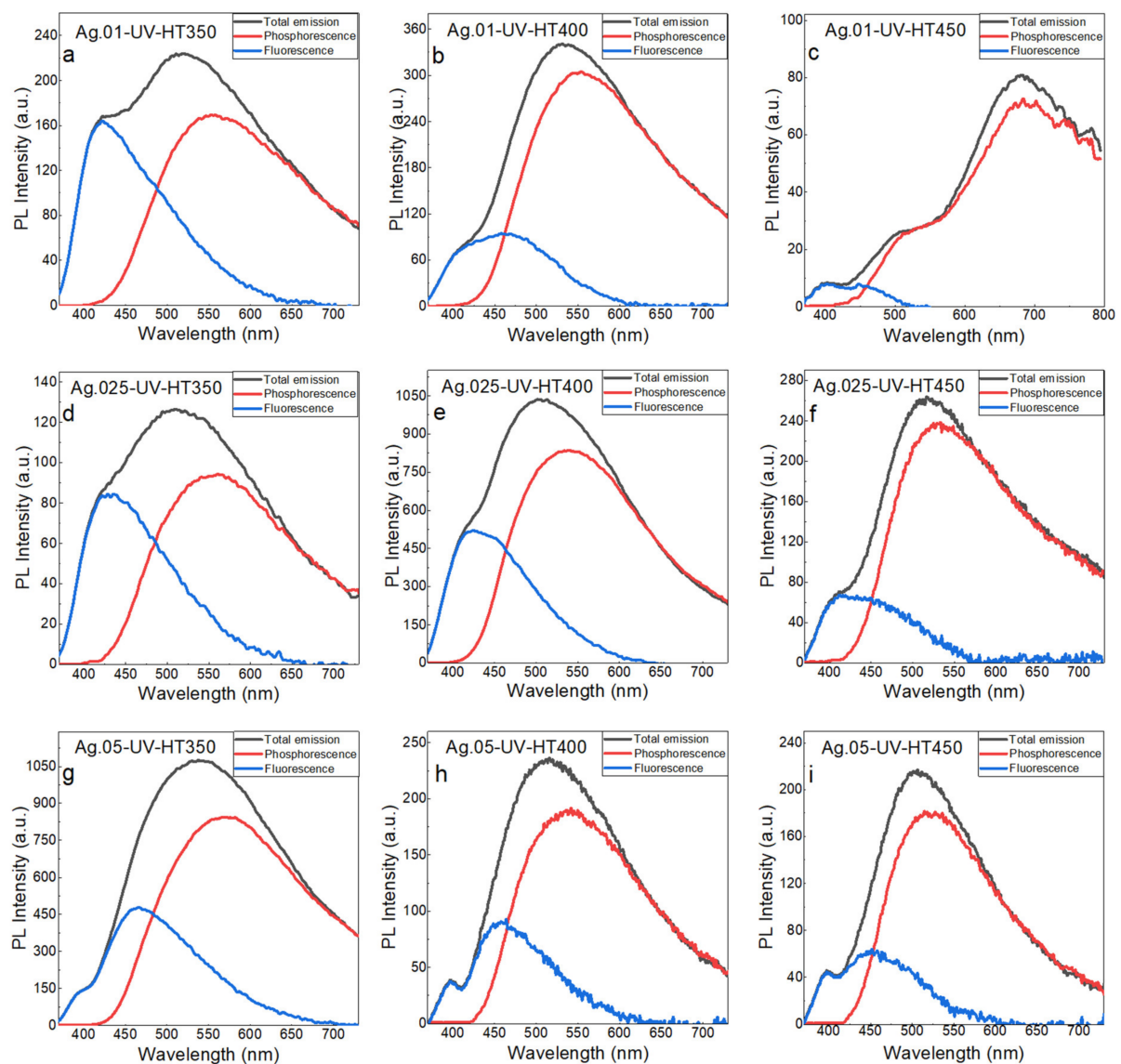


**Figure 3.** Fluorescence, phosphorescence, and total emission spectra of Ag.01 glass after UV irradiation and heat treatment at (a) 350, (b) 400, and (c) 450 °C. Fluorescence, phosphorescence, and total emission spectra of Ag.025 glass after UV irradiation and heat treatment at (d) 350, (e) 400, and (f) 450 °C. Fluorescence, phosphorescence, and total emission spectra of Ag.05 glass after UV irradiation and heat treatment at (g) 350, (h) 400, and (i) 450 °C. All spectra were measured with  $\lambda_{\text{ex}} = 340$  nm.

Although the heat-treated samples of Ag.05 glass manifested clear plasmon absorption bands, the emission of silver clusters in these samples was not quenched. The photoluminescence quantum yield of the Ag.05 sample heat treated at 400 °C reached the maximum observed value of 0.43 (Table 2). This result indicates that luminescent silver clusters and plasmonic nanoparticles can coexist in glass without negative effects on the emissive properties of the clusters. It has been shown that a characteristic emission of silver clusters was observed for Ag.05 glass right after synthesis (Figure 2a); further development of the effective cluster luminescence after UV irradiation and heat treatment implies that a significant part of silver in glass did not form plasmonic nanoparticles and remained in the form of  $\text{Ag}^+$  ions. The fluorescence and phosphorescence lifetimes (Table 3), as well as the spectral properties (Figure 3), were the same for all heat-treated samples, except for the Ag.01 sample after heat treatment at 450 °C. Average fluorescence lifetimes coincided within 0.5 ns, and phosphorescence lifetimes had values of 120–141  $\mu\text{s}$ . Unlike the lifetimes of emission, quantum yields of luminescence differed by more than a factor of two, from

0.16 to 0.43. Considering that the applied method of quantum yield measurements determines the external quantum efficiency, this significant difference should originate from the existence of passive absorption at the excitation wavelength. Possible sources of passive absorption are plasmonic nanoparticles and other non-luminescent silver species, as well as the residual  $Ce^{3+}$  ions. To evaluate the possible application of the studied glass samples for the generation of white light, CIE chromaticity coordinates were calculated for the selected glass samples (Figure 4b).

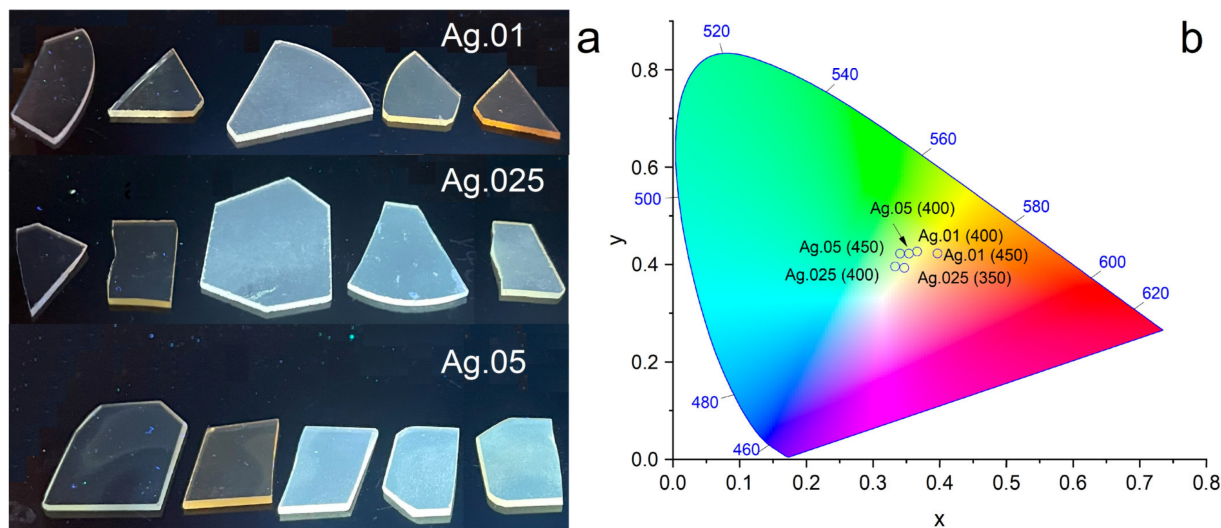


**Figure 4.** Photo of initial, UV-irradiated, and heat-treated glass samples at temperatures 350, 400, and 450 °C (from left to right) under UV illumination (a). CIE chromaticity diagram of the selected glass samples. Temperatures of heat treatment are presented in brackets (b).

**Table 3.** Fluorescence and phosphorescence lifetimes of Ag.01, Ag.025, and Ag.05 glass samples under 340 nm excitation.  $\tau_{f\_avg}$ —average fluorescence lifetime registered at  $\lambda_{em} = 405$  nm for initial glasses and  $\lambda_{em} = 400$  nm for heat-treated glasses,  $\tau_p$ —phosphorescence lifetime measured at  $\lambda_{em} = 485$  nm for initial Ag.05 glass and  $\lambda_{em} = 515$  nm for heat-treated glasses.

Heat Treatment Temperature, °C	Ag.01		Ag.025		Ag.05	
	$\tau_{f\_avg}$ (ns)	$\tau_p$ ( $\mu$ s)	$\tau_{f\_avg}$ (ns)	$\tau_p$ ( $\mu$ s)	$\tau_{f\_avg}$ (ns)	$\tau_p$ ( $\mu$ s)
Initial glass	23.7	-	28.3	-	16.9	100
350	3.7	141	3.2	132	3.3	135
400	3.6	136	3.4	136	3.4	133
450	4.5	105	3.2	123	3.4	120

Based on the spectroscopic characterization of the synthesized glass samples, we have chosen Ag.01 glass after heat treatment at 350 °C and Ag.025 glass after heat treatment at 400 °C for the analysis of photophysical process rates. The chosen samples had the highest quantum yields of luminescence for a given concentration of  $Ag_2O$  and demonstrated no spectral features of plasmonic nanoparticles. The rate constants of cluster fluorescence, phosphorescence, and intersystem crossing were estimated on the basis of the earlier proposed approach [40], which is summarized below. It was supposed that a set of silver clusters formed in the glass is responsible for the bright white luminescence under near-UV excitation. Broad emission spectra originate from inhomogeneous broadening by different local environments in the glass matrix. Based on the observed fluorescence and phosphorescence emission components, a three-level energy diagram with the ground singlet state  $S_0$ , excited singlet  $S_1$ , and triplet  $T_1$  states (Figure 5a) was applied to analyze the photophysics of silver clusters in glass. After photoexcitation of a silver cluster, the  $S_1$  state



is deactivated radiatively via fluorescence with the process rate constant  $k_f$  or nonradiatively via intersystem crossing with the process rate constant  $k_{isc}$ . The probability of direct  $S_1$  deactivation via internal conversion is negligible, since the energy of the fluorescence transition is significantly higher than the typical phonon energy of silicate glass [41]. After the intersystem crossing, the excited triplet state  $T_1$  is deactivated radiatively via phosphorescence with the process rate constant  $k_p$  or nonradiatively with the rate constant  $k_{nrT}$ . Similar three-level energy diagrams were used to describe the properties of silver clusters in other glass systems [42,43]. Within the used approach, it was necessary to measure the quantum yield of emission, separate the spectra of fluorescence and phosphorescence, and the emission yield decays of fluorescence and phosphorescence to estimate the rate constants of silver clusters. It is important to note that the applied method of photophysical process rate determination provides average values of the rate constants, while the properties of a single silver cluster may deviate from them.

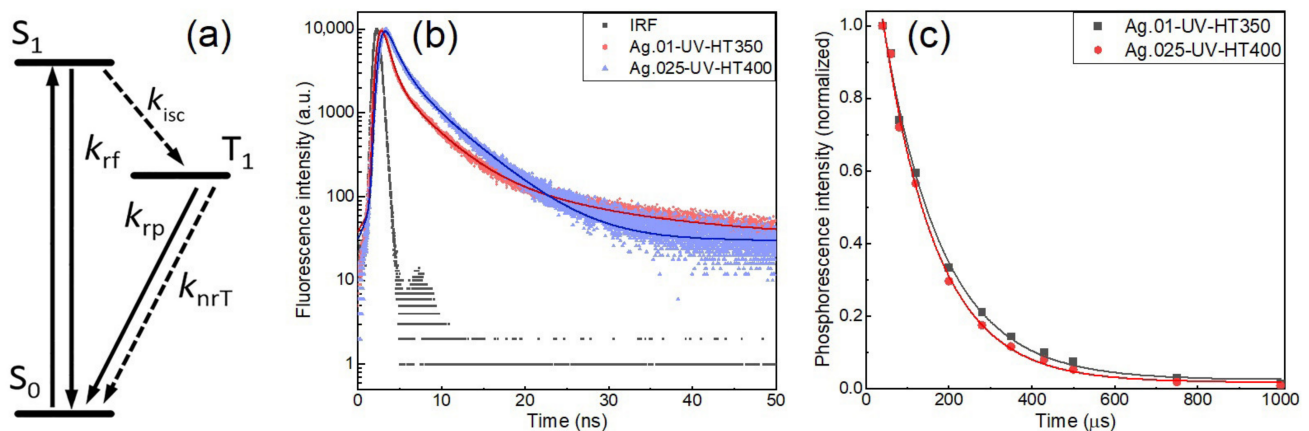


**Figure 5.** Energy level diagram of silver clusters.  $k_{rf}$  and  $k_{rp}$ —radiative rate constants of fluorescence and phosphorescence,  $k_{isc}$ —intersystem crossing rate constant,  $k_{nrT}$ —nonradiative deactivation of the triplet state rate constant (a). Fluorescence decay curves of the Ag.01 glass after UV irradiation and heat treatment at 350 °C and Ag.05 glass after UV irradiation and heat treatment at 400 °C measured at  $\lambda_{em} = 400$  nm,  $\lambda_{ex} = 340$  nm (b). Phosphorescence decay curves of the Ag.01 glass after UV irradiation and heat treatment at 350 °C and Ag.05 glass after UV irradiation and heat treatment at 400 °C measured at  $\lambda_{em} = 515$  nm,  $\lambda_{ex} = 340$  nm (c).

Figure 5b,c demonstrate the decay curves of fluorescence and phosphorescence. The corresponding lifetimes used for estimation of the photophysical parameters of silver clusters and luminescence quantum yields are summarized in Table 4. Comparison of the luminescence quantum yields and emission lifetimes obtained for silver clusters in the bulk of glass with earlier published results on silver clusters formed by ion exchange in the same glass matrix shows that no significant difference between these synthesis approaches is observed. The most prominent difference in the value of luminescence quantum yield partly originates from the passive absorption at the excitation wavelength since the formation of clusters in ion-exchange layers does not require the cerium in glass composition. The ion exchange procedure used to form silver clusters in photo-thermo-refractive glass provides an average  $Ag_2O$  concentration of 5.2 mol.% in a 12.4  $\mu m$  layer with a surface concentration of 12.7 mol.% [24]. Therefore, the concentrations of silver ions used to form luminescent silver clusters in the glass bulk were 200–500 times lower than in the ion exchange method. Nevertheless, those great differences in the concentration of  $Ag^+$  ions in glass do not lead to the formation of fundamentally different emissive silver clusters. Analysis of the rate constants of photophysical processes shows that a common feature of silver clusters in photo-thermo-refractive glass is a very fast intersystem crossing, leading to the prevalence of phosphorescence in the emission (Table 5). The radiative rate constants of fluorescence



and phosphorescence are of the same order of magnitude, as well as the constant rates of the triplet state deactivation.

**Table 4.** Photophysical parameters of silver clusters in Ag.01 glass after UV irradiation and heat treatment at 350 °C and Ag.05 glass after UV irradiation and heat treatment at 400 °C.  $\tau_1$ —lifetime of *i* fluorescence component,  $\tau_{f\_avg}$ —average fluorescence lifetime registered at  $\lambda_{em} = 400$  nm,  $\tau_p$ —phosphorescence lifetime measured at  $\lambda_{em} = 515$  nm. All lifetimes were measured with  $\lambda_{ex} = 340$  nm.  $\Phi_{lum}$ —luminescence quantum yield of glass samples under 340 nm excitation.

Sample	$\tau_1$ , ns	$\tau_2$ , ns	$\tau_3$ , ns	$\tau_{f\_avg}$ , ns	$\tau_p$ , $\mu$ s	$\Phi_{lum}$	Reference
Ag.01-UV-HT350	0.8	3.8	14.5	3.7	141	0.25	this work
Ag.025-UV-HT400	1.3	5.1	-	3.4	136	0.42	this work
Ion-exchanged sample	1.5	5.0	-	3.8	110	0.66	[40]

**Table 5.** Photophysical parameters of silver clusters in Ag.01 glass after UV irradiation and heat treatment at 350 °C and Ag.05 glass after UV irradiation and heat treatment at 400 °C.  $k_{rf}$  and  $k_{rp}$ —radiative rate constants of fluorescence and phosphorescence,  $k_{isc}$ —intersystem crossing rate constant,  $k_{nrT}$ —nonradiative deactivation of the triplet state rate constant,  $\Phi_f$ ,  $\Phi_{isc}$ , and  $\Phi_p$ —fluorescence, intersystem crossing, and phosphorescence quantum yields.

Sample	$k_{rf}$ ( $s^{-1}$ )	$k_{isc}$ ( $s^{-1}$ )	$k_{rp}$ ( $s^{-1}$ )	$k_{nrT}$ ( $s^{-1}$ )	$\Phi_f$	$\Phi_{isc}$	$\Phi_p$	Reference
Ag.01-UV-HT350	$1.6 \cdot 10^7$	$2.5 \cdot 10^8$	$1.4 \cdot 10^3$	$5.6 \cdot 10^3$	0.06	0.94	0.20	this work
Ag.025-UV-HT400	$2.3 \cdot 10^7$	$2.7 \cdot 10^8$	$2.7 \cdot 10^3$	$4.6 \cdot 10^3$	0.08	0.92	0.37	this work
Ion-exchanged sample	$3.2 \cdot 10^7$	$2.3 \cdot 10^8$	$5.6 \cdot 10^3$	$3.6 \cdot 10^3$	0.12	0.88	0.61	[40]

#### 4. Conclusions

Luminescent silver clusters were formed in the bulk of photo-thermo-refractive glass containing 0.01, 0.025, and 0.05 mol.% of Ag<sub>2</sub>O. Spontaneous formation of plasmonic nanoparticles during glass synthesis was observed at 0.05 mol.% of Ag<sub>2</sub>O in the glass composition. After UV irradiation and heat treatment of the synthesized glasses, efficient formation of silver clusters with bright white luminescence was observed even for the glass samples with plasmonic nanoparticles. The spectroscopic characterization using steady-state and time-resolved techniques revealed that silver clusters in the glass bulk have the same characteristic features as the previously studied silver clusters in ion-exchange layers. The emission spectra of silver clusters consist of fluorescence with an average lifetime of 3.2–4.5 ns and phosphorescence with a lifetime of 105–141  $\mu$ s. The quantum yield of the studied glass samples varies from 0.25 to 0.42. Based on experimental studies, the estimation of the radiative rate constants of fluorescence and phosphorescence, the rate constant of intersystem crossing, and the rate constant of nonradiative deactivation of the triplet state was performed. The results obtained on fluorescence and phosphorescence lifetimes and quantum yields, as well as the rates of photophysical processes, were compared with the previously obtained results for silver clusters formed in ion-exchange layers of the same glass matrix. It was revealed that different synthesis approaches form close sets of emissive silver clusters, despite the difference in Ag<sup>+</sup> concentration by 200–500 times. This result suggests that silver clusters of one type are responsible for the white emission of the studied glasses.

**Author Contributions:** Formal analysis, L.Y.M.; Investigation, L.Y.M., D.V.M., M.D.S., K.S.Z., A.A.S. and I.E.K.; Writing—original draft, L.Y.M.; Writing—review and editing, L.Y.M. All authors have read and agreed to the published version of the manuscript.

**Funding:** This research was funded by the Russian Science Foundation, project NO 22-73-10055.

**Institutional Review Board Statement:** Not applicable.

**Informed Consent Statement:** Not applicable.

**Data Availability Statement:** The data presented in this study are available on request from the corresponding author.

**Acknowledgments:** Fluorescence decay measurements were carried out in the 'Center for Optical and Laser materials research' (Saint Petersburg State University).

**Conflicts of Interest:** The authors declare no conflict of interest.

## References

1. Kuznetsov, A.S.; Tikhomirov, V.K.; Shestakov, M.V.; Moshchalkov, V.V. Ag Nanocluster Functionalized Glasses for Efficient Photonic Conversion in Light Sources, Solar Cells and Flexible Screen Monitors. *Nanoscale* **2013**, *5*, 10065–10075. [[CrossRef](#)] [[PubMed](#)]
2. Tan, D.; Jiang, P.; Xu, B.; Qiu, J. Single-Pulse-Induced Ultrafast Spatial Clustering of Metal in Glass: Fine Tunability and Application. *Adv. Photonics Res.* **2021**, *2*, 2000121. [[CrossRef](#)]
3. Wu, Y.; Lin, H.; Li, R.; Lin, S.; Wu, C.; Huang, Q.; Xu, J.; Cheng, Y.; Wang, Y. Laser-Direct-Writing of Molecule-like  $\text{Ag}_m^{x+}$  nanoclusters in Transparent Tellurite Glass for 3D Volumetric Optical Storage. *Nanoscale* **2021**, *13*, 19663–19670. [[CrossRef](#)] [[PubMed](#)]
4. De Cremer, G.; Sels, B.F.; Hotta, J.I.; Roeffaers, M.B.J.; Bartholomeeusen, E.; Coutiño-Gonzalez, E.; Valtchev, V.; De Vos, D.E.; Vosch, T.; Hofkens, J. Optical Encoding of Silver Zeolite Microcarriers. *Adv. Mater.* **2010**, *22*, 957–960. [[CrossRef](#)]
5. Dong, X.Y.; Si, Y.; Yang, J.S.; Zhang, C.; Han, Z.; Luo, P.; Wang, Z.Y.; Zang, S.Q.; Mak, T.C.W. Ligand Engineering to Achieve Enhanced Ratiometric Oxygen Sensing in a Silver Cluster-Based Metal-Organic Framework. *Nat. Commun.* **2020**, *11*, 3678. [[CrossRef](#)]
6. Qian, S.; Wang, Z.; Zuo, Z.; Wang, X.; Wang, Q.; Yuan, X. Engineering Luminescent Metal Nanoclusters for Sensing Applications. *Coord. Chem. Rev.* **2022**, *451*, 214268. [[CrossRef](#)]
7. Zheng, W.; Li, P.; Wang, C.; Qiao, X.; Qian, G.; Fan, X. Tuning Ag Quantum Clusters in Glass as an Efficient Spectral Converter: From Fundamental to Applicable. *J. Non. Cryst. Solids* **2023**, *599*, 121910. [[CrossRef](#)]
8. Fares, H.; Santos, S.N.C.; Santos, M.V.; Franco, D.F.; Souza, A.E.; Manzani, D.; Mendonça, C.R.; Nalin, M. Highly Luminescent Silver Nanocluster-Doped Fluorophosphate Glasses for Microfabrication of 3D Waveguides. *RSC Adv.* **2017**, *7*, 55935–55944. [[CrossRef](#)]
9. Aslani, M.; Talebi, R.; Vashaee, D. Coupling Light in Ion-Exchanged Waveguides by Silver Nanoparticle-Based Nanogratings: Manipulating the Refractive Index of Waveguides. *ACS Appl. Nano Mater.* **2022**, *5*, 5439–5447. [[CrossRef](#)]
10. de Castro, T.; Fares, H.; Khalil, A.A.; Laberdesque, R.; Petit, Y.; Strutinski, C.; Danto, S.; Jubera, V.; Ribeiro, S.J.L.; Nalin, M.; et al. Femtosecond Laser Micro-Patterning of Optical Properties and Functionalities in Novel Photosensitive Silver-Containing Fluorophosphate Glasses. *J. Non. Cryst. Solids* **2019**, *517*, 51–56. [[CrossRef](#)]
11. Sholom, S.; McKeever, S.W.S. Silver Molecular Clusters and the Properties of Radiophotoluminescence of Alkali-Phosphate Glasses at High Dose. *Radiat. Meas.* **2023**, *163*, 106924. [[CrossRef](#)]
12. McKeever, S.W.S.; Sholom, S.; Shrestha, N.; Klein, D.M. Build-up of Radiophotoluminescence (RPL) in Ag-Doped Phosphate Glass in Real-Time Both during and after Exposure to Ionizing Radiation: A Proposed Model. *Radiat. Meas.* **2020**, *132*, 106246. [[CrossRef](#)]
13. Han, Z.; Dong, X.Y.; Luo, P.; Li, S.; Wang, Z.Y.; Zang, S.Q.; Mak, T.C.W. Ultrastable Atomically Precise Chiral Silver Clusters with More than 95% Quantum Efficiency. *Sci. Adv.* **2020**, *6*, eaay0107. [[CrossRef](#)]
14. Cho, J.; Park, J.H.; Kim, J.K.; Schubert, E.F. White Light-Emitting Diodes: History, Progress, and Future. *Laser Photonics Rev.* **2017**, *11*, 1600147. [[CrossRef](#)]
15. Grandjean, D.; Coutiño-Gonzalez, E.; Cuong, N.T.; Fron, E.; Baekelant, W.; Aghakhani, S.; Schlexer, P.; D'Acapito, F.; Banerjee, D.; Roeffaers, M.B.J.; et al. Origin of the Bright Photoluminescence of Few-Atom Silver Clusters Confined in LTA Zeolites. *Science* **2018**, *361*, 686–690. [[CrossRef](#)]
16. Coutiño-Gonzalez, E.; Baekelant, W.; Grandjean, D.; Roeffaers, M.B.J.; Fron, E.; Aghakhani, M.S.; Bovet, N.; Van Der Auweraer, M.; Lievens, P.; Vosch, T.; et al. Thermally Activated LTA(Li)-Ag Zeolites with Water-Responsive Photoluminescence Properties. *J. Mater. Chem. C* **2015**, *3*, 11857–11867. [[CrossRef](#)]
17. Baekelant, W.; Aghakhani, S.; Fron, E.; Martin, C.; Woong-Kim, C.; Steele, J.A.; De Baerdemaeker, T.; D'Acapito, F.; Chernysov, D.; Van Der Auweraer, M.; et al. Luminescent Silver-Lithium-Zeolite Phosphors for near-Ultraviolet LED Applications. *J. Mater. Chem. C* **2019**, *7*, 14366–14374. [[CrossRef](#)]

18. Fenwick, O.; Coutiño-Gonzalez, E.; Grandjean, D.; Baekelant, W.; Richard, F.; Bonacchi, S.; De Vos, D.; Lievens, P.; Roeffaers, M.; Hofkens, J.; et al. Tuning the Energetics and Tailoring the Optical Properties of Silver Clusters Confined in Zeolites. *Nat. Mater.* **2016**, *15*, 1017–1022. [[CrossRef](#)]
19. Coutino-Gonzalez, E.; Roeffaers, M.B.J.; Dieu, B.; De Cremer, G.; Leyre, S.; Hanselaer, P.; Fyen, W.; Sels, B.; Hofkens, J. Determination and Optimization of the Luminescence External Quantum Efficiency of Silver-Clusters Zeolite Composites. *J. Phys. Chem. C* **2013**, *117*, 6998–7004. [[CrossRef](#)]
20. Kuznetsov, A.S.; Tikhomirov, V.K.; Moshchalkov, V.V. UV-Driven Efficient White Light Generation by Ag Nanoclusters Dispersed in Glass Host. *Mater. Lett.* **2013**, *92*, 4–6. [[CrossRef](#)]
21. Hu, T.; Zheng, W.; Liu, Z.; Jia, J.; Xu, X.; Xu, Q.; Qiao, X.; Fan, X. Strategies to Host Silver Quantum Clusters in Borosilicate Glass: How to Mutually Fulfill PL Efficiency and Chemical Stability? *J. Non-Crystalline Solids X* **2022**, *16*, 100132. [[CrossRef](#)]
22. Sgibnev, Y.M.; Nikonorov, N.V.; Ignatiev, A.I. High Efficient Luminescence of Silver Clusters in Ion-Exchanged Antimony-Doped Photo-Thermo-Refractive Glasses: Influence of Antimony Content and Heat Treatment Parameters. *J. Lumin.* **2017**, *188*, 172–179. [[CrossRef](#)]
23. Dubrovin, V.D.; Ignatiev, A.I.; Nikonorov, N.V.; Sidorov, A.I.; Shakhverdov, T.A.; Agafonova, D.S. Luminescence of Silver Molecular Clusters in Photo-Thermo-Refractive Glasses. *Opt. Mater.* **2014**, *36*, 753–759. [[CrossRef](#)]
24. Mironov, L.Y.; Marasanov, D.V.; Ulshina, M.D.; Sgibnev, Y.M.; Kolesnikov, I.E.; Nikonorov, N.V. The Role of Thermally Activated Quenching and Energy Migration in Luminescence of Silver Clusters in Glasses. *J. Phys. Chem. C* **2022**, *126*, 13863–13869. [[CrossRef](#)]
25. West, B.R. Ion-Exchanged Glass Waveguide Technology: A Review. *Opt. Eng.* **2011**, *50*, 071107. [[CrossRef](#)]
26. Stepanov, A.L.; Hole, D.E.; Townsend, P.D. Formation of Silver Nanoparticles in Soda-Lime Silicate Glass by Ion Implantation near Room Temperature. *J. Non. Cryst. Solids* **1999**, *260*, 65–74. [[CrossRef](#)]
27. Arnold, G.W.; Borders, J.A. Aggregation and Migration of Ion-implanted Silver in Lithia-alumina-silica Glass. *J. Appl. Phys.* **1977**, *48*, 1488–1496. [[CrossRef](#)]
28. Lumeau, J.; Zanotto, E.D. A Review of the Photo-Thermal Mechanism and Crystallization of Photo-Thermo-Refractive (PTR) Glass. *Int. Mater. Rev.* **2017**, *62*, 348–366. [[CrossRef](#)]
29. Ivanov, S.; Dubrovin, V.; Nikonorov, N.; Stolyarchuk, M.; Ignatiev, A. Origin of Refractive Index Change in Photo-Thermo-Refractive Glass. *J. Non. Cryst. Solids* **2019**, *521*, 119496. [[CrossRef](#)]
30. Efimov, A.M.; Ignatiev, A.I.; Nikonorov, N.V.; Postnikov, E.S. Quantitative UV-VIS Spectroscopic Studies of Photo-Thermo-Refractive Glasses. II. Manifestations of Ce<sup>3+</sup> and Ce(IV) Valence States in the UV Absorption Spectrum of Cerium-Doped Photo-Thermo-Refractive Matrix Glasses. *J. Non. Cryst. Solids* **2013**, *361*, 26–37. [[CrossRef](#)]
31. Paul, A.; Mulholland, M.; Zaman, M.S. Ultraviolet Absorption of Cerium(III) and Cerium(IV) in Some Simple Glasses. *J. Mater. Sci.* **1976**, *11*, 2082–2086. [[CrossRef](#)]
32. Hövel, H.; Fritz, S.; Hilger, A.; Kreibitz, U.; Vollmer, M. Width of Cluster Plasmon Resonances: Bulk Dielectric Functions and Chemical Interface Damping. *Phys. Rev. B* **1993**, *48*, 18178–18188. [[CrossRef](#)]
33. Arnold, G.W. Near-surface Nucleation and Crystallization of an Ion-implanted Lithia-alumina-silica Glass. *J. Appl. Phys.* **1975**, *46*, 4466–4473. [[CrossRef](#)]
34. Jiménez, J.A.; Sendova, M.; Liu, H. Evolution of the Optical Properties of a Silver-Doped Phosphate Glass during Thermal Treatment. *J. Lumin.* **2011**, *131*, 535–538. [[CrossRef](#)]
35. Sontakke, A.D.; Ueda, J.; Tanabe, S. Effect of Synthesis Conditions on Ce<sup>3+</sup> Luminescence in Borate Glasses. *J. Non. Cryst. Solids* **2016**, *431*, 150–153. [[CrossRef](#)]
36. Chewpraditkul, W.; Shen, Y.; Chen, D.; Yu, B.; Prusa, P.; Nikl, M.; Beitlerova, A.; Wanarak, C. Luminescence and Scintillation of Ce<sup>3+</sup>-Doped High Silica Glass. *Opt. Mater.* **2012**, *34*, 1762–1766. [[CrossRef](#)]
37. Mironov, L.Y.; Marasanov, D.V.; Sgibnev, Y.M.; Sannikova, M.D.; Kulpina, E. V Influence of Reducing Agent Concentration on the Luminescence and Photophysical Processes Constant Rates of Silver Clusters in Silica-Based Glass. *J. Lumin.* **2023**, *261*, 119918. [[CrossRef](#)]
38. He, Y.; Pei, G.; Liu, J.; Fang, Z.; Wang, L.; Jiang, S.; Yu, B.; Gou, J.; Liu, S.F. Utilizing the Energy Transfer of Ce<sup>4+</sup>- and Ce<sup>3+</sup>-Tb<sup>3+</sup> to Boost the Luminescence Quantum Efficiency up to 100% in Borate Glass. *J. Phys. Chem. C* **2022**, *126*, 5838–5846. [[CrossRef](#)]
39. Efimov, A.M.; Ignatiev, A.I.; Nikonorov, N.V.; Postnikov, E.S. Quantitative UV-VIS Spectroscopic Studies of Photo-Thermo-Refractive Glasses. I. Intrinsic, Bromine-Related, and Impurity-Related UV Absorption in Photo-Thermo-Refractive Glass Matrices. *J. Non. Cryst. Solids* **2011**, *357*, 3500–3512. [[CrossRef](#)]
40. Marasanov, D.V.; Mironov, L.Y.; Sgibnev, Y.M.; Kolesnikov, I.E.; Nikonorov, N.V. Luminescence and Energy Transfer Mechanisms in Photo-Thermo-Refractive Glasses Co-Doped with Silver Molecular Clusters and Eu<sup>3+</sup>. *Phys. Chem. Chem. Phys.* **2020**, *22*, 23342–23350. [[CrossRef](#)]
41. Cao, R.; Lu, Y.; Tian, Y.; Huang, F.; Guo, Y.; Xu, S.; Zhang, J. 2 Mm Emission Properties and Nonresonant Energy Transfer of Er<sup>3+</sup> and Ho<sup>3+</sup> Codoped Silicate Glasses. *Sci. Rep.* **2016**, *6*, 37873. [[CrossRef](#)] [[PubMed](#)]

42. Zheng, W.; Zhou, B.; Ren, Z.; Xu, X.; Yang, G.; Qiao, X.; Yan, D.; Qian, G.; Fan, X. Fluorescence–Phosphorescence Manipulation and Atom Probe Observation of Fully Inorganic Silver Quantum Clusters: Imitating from and Behaving beyond Organic Hosts. *Adv. Opt. Mater.* **2022**, *10*, 2101632. [[CrossRef](#)]
43. Li, L.; Yang, Y.; Zhou, D.; Yang, Z.; Xu, X.; Qiu, J. Influence of the  $\text{Eu}^{2+}$  on the Silver Aggregates Formation in  $\text{Ag}^+$ - $\text{Na}^+$  Ion-Exchanged  $\text{Eu}^{3+}$ -Doped Sodium-Aluminosilicate Glasses. *J. Am. Ceram. Soc.* **2014**, *97*, 1110–1114. [[CrossRef](#)]

**Disclaimer/Publisher’s Note:** The statements, opinions and data contained in all publications are solely those of the individual author(s) and contributor(s) and not of MDPI and/or the editor(s). MDPI and/or the editor(s) disclaim responsibility for any injury to people or property resulting from any ideas, methods, instructions or products referred to in the content.